

1 \leftrightarrow 2 Processes of a Sterile Neutrino Around Electroweak Scale in the Thermal Plasma

Xue-Min Jiang, Yi-Lei Tang,^{*} Zhao-Huan Yu, and Hong-Hao Zhang[†]
School of Physics, Sun Yat-Sen University, Guangzhou 510275, China

(Dated: August 4, 2020)

Abstract

In this paper, we will apply the Goldstone equivalence gauge to calculate the 1 \leftrightarrow 2 processes of a sterile neutrino in the thermal plasma below the standard model (SM) critical temperature $T_c \approx 160$ GeV. The sterile neutrino's mass is around the electroweak scale $50 \text{ GeV} \leq m_N \leq 200 \text{ GeV}$, and the acquired thermal averaged effective width $\bar{\Gamma}_{\text{tot}}$ is continuous around the cross-over. We will also apply our results to perform a preliminary calculation of the leptogenesis.

PACS numbers:

arXiv:2008.00642v1 [hep-ph] 3 Aug 2020

^{*}tangylei@mail.sysu.edu.cn

[†]zhh98@mail.sysu.edu.cn

I. INTRODUCTION

Sterile neutrinos interacting with the plasma background of the early universe can become a potential solution to some cosmic particle physics problems. A prominent example is the Leptogenesis[1]. The CP-violation effects of the sterile neutrino's interactions with the light leptons give rise to the lepton number asymmetry in the plasma, and the baryon number asymmetry accordingly appears through the sphaleron effects(For some early works, see [2–6], and see [7–10] for reviews.). The sterile neutrino can also become a portal to the dark matter. Being a variation of a secluded dark matter model, a “sterile neutrino philic dark matter” model[11–18] gives a different relic density result compared with the standard weakly interacting massive particle (WIMP) models[19]. In Ref. [20], we also studied a feebly interacting massive particle (FIMP)[21] version of such kind of models. Sometimes, sterile neutrinos themselves can also become the dark matter candidate. Among all these examples, a reliable calculation of a sterile neutrino's interaction with the thermal plasma is very crucial for the precise predictions of their physical observables compared with the experimental data.

When $m_N \gg T_c \simeq 160\text{GeV}$, where m_N is the sterile neutrino mass and T_c is the electroweak cross-over temperature[22], there are plenty of reliable discussions in the literature to calculate the sterile neutrino's production[23–31], since the crucial temperature $T \sim m_N$ is well above the cross-over temperature, only the Higgs doublet and the active leptons participate the $1 \leftrightarrow 2$ processes. The Higgs components receive a universal thermal mass correction, which is easy to calculate. For lighter sterile neutrinos, successful leptogenesis can also be acquired through the resonant effects[32–38]. When $m_N \ll T_c$, at $T \sim m_N \ll T_c$, the thermal mass terms can be safely neglected since the vacuum expectation value (vev) of the Higgs boson becomes fairly close to the zero-temperature value ~ 246 GeV, and the boson's behaviours are similar to those in the zero-temperature situation[39].

In the literature, there seems to be a gap when $m_N \sim T_c$. In this range the calculation is plagued by the intricate thermal corrections to the gauge and Higgs sectors. In Ref. [40], the authors estimated the the $U(1)_Y \times SU(2)_L$ gauge boson contributions by replacing them with the Goldstone degrees of freedom artificially assigned with the similar mass of the Higgs boson. We also applied this method in the corresponding calculations of our papers [12, 20]. Such an ansatz method might be inspired by the famous “Goldstone equivalence theorem” in

the zero temperature, which requires more investigations in the thermal plasma case. A safe procedure is to return to the original form of the finite temperature propagators to integrate all the branch cuts and poles whatever appear, as described in Ref. [41–44]. However, it is formidable for one to follow the procedures there, and the relationship between the Goldstone and gauge boson becomes more obscure. Another fact is that the invariant squared mass of the sterile neutrino, which is denoted by \mathcal{K}^2 in Ref. [41–44], had been neglected around T_c there, so their method is not suitable to our interested $\mathcal{K}^2 = m_N^2 \sim T_c^2$ range.

In Ref. [45] we proposed a method to decompose the massive gauge boson propagators in the thermal plasma. Poles indicating the “transverse” and “longitudinal” degree of freedom arise as usual, and a branch cut which extremely resembles two massless poles was identified as the “cadaver” of the Goldstone boson. When $T > T_c$, such a branch cut fragments into two actual poles corresponding to the Goldstone boson particles, and when $T = 0$, this branch cut completely disappears. In the finite temperature, the longitudinal polarization is also some intermediate state between the so-called “plasmon” and the Goldstone equivalent state. We made an analogy that the longitudinal polarization will “spew out” a fraction of the Goldstone’s cadaver in the finite temperature’s environment. This helps us include all the contributions from the transverse, longitudinal, Higgs and Goldstone degrees of freedom correctly, and help us clarify the relationship between the Goldstone and the gauge boson in the plasma.

In this paper, with the method we have developed in Ref. [45], we will calculate the sterile neutrino $1 \leftrightarrow 2$ processes near the electroweak cross-over temperature $m_N \sim T \sim T_c$. We will also roughly discuss the leptogenesis induced by these processes. A complete calculation of a sterile neutrino’s interaction in the early universe should also include the more complicated $2 \leftrightarrow 2$ scattering processes. In many cases when $T \gg m_N$, and the l - H - N Yukawa couplings $y_N \gtrsim 10^{-8}$ which are sufficiently large, thermal equilibrium of the sterile neutrino does not require a detailed calculation. When the temperature drops to the $T \sim m_N$ scale, the out-of-equilibrium effects start to arise, and these $2 \leftrightarrow 2$ processes are usually suppressed rapidly due to an additional number density factor compared with the $1 \leftrightarrow 2$ processes. With these considerations, we leave the $2 \leftrightarrow 2$ processes in our future study and do not consider their contributions on this stage. We also do not consider the contributions resumming the interchange/emission of the soft bosons[46–48] in this paper for brevity and simplicity.

II. BASIC CONCEPTS AND CHANNEL ENUMERATION

The Lagrangian of sterile neutrino is the standard one

$$\mathcal{L} \supset \mathcal{L}_{\text{SM}} + \mathcal{L}_{\text{N kin}} + \mathcal{L}_{\text{N mass}} + \sqrt{2}y_{Nij}H\bar{l}_iN_j + \text{h.c.}, \quad (1)$$

where H is the Higgs doublet, L_i , $i = 1, 2, 3$ is the lepton doublet of three generations, N_j are the sterile neutrinos. N_j can be either Majorana or (pseudo-)Dirac spinors, and the corresponding kinematical and mass terms $\mathcal{L}_{\text{N kin}} + \mathcal{L}_{\text{N mass}}$ differ by a factor of $\frac{1}{2}$. For simplicity here we only study the one Dirac sterile neutrino case. The interaction only involves one massless lepton. A general situation can be inferred from our results by simply multiplying some factors. Therefore, the Lagrangian we are relying on is given by

$$\mathcal{L} \supset \mathcal{L}_{\text{SM}} - i\bar{N}\not{\partial}N + m_N\bar{N}N + \sqrt{2}y_NH\bar{l}N + \text{h.c.}, \quad (2)$$

where m_N is the mass of the sterile neutrino.

Above the standard model (SM) critical temperature of the cross-over $T > T_c \approx 160$ GeV, the $1 \leftrightarrow 2$ processes of the sterile neutrino has nothing to do with the W/Z boson. Only the Higgs doublets including the Goldstone components participate the couplings. The whole process is quite standard: the thermal effects correct the effective Higgs mass term

$$\delta m_{H, \text{thermal}}^2 = (g_1^2 + 3g_2^2 + 4y_t^2 + 8\lambda)\frac{T^2}{16}, \quad (3)$$

where g_1 , g_2 are the electroweak gauge coupling constants, y_t is the top Yukawa coupling constant, and the λ is the 4-Higgs coupling constant. Leptons also receive the thermal mass corrections. In the thermal plasma, each pole in the leptonic propagators are split into two objects, so called a ‘‘particle’’ and a ‘‘hole’’. In the Ref. [23], both these two objects are combined into one single particle with the universal thermal mass correction to estimate the phase space. In this paper, we abandon this approximation, and earnestly sum over each contributions from these two degrees of freedom.

Below the critical temperature $T < T_c$, the vacuum expectation value (vev) is estimated to be $v(T) = v_0\sqrt{1 - \frac{T^2}{T_c^2}}$, where $v_0 = 246$ GeV. This opens the the sterile neutrino’s oscillation into a highly off-shell active neutrino, and then it decays into a W/Z gauge boson plus a charged lepton/active neutrino. An on-shell W/Z boson can also decay into a pair of leptons, and the active neutrino product can also oscillate into a sterile neutrino through the vev.

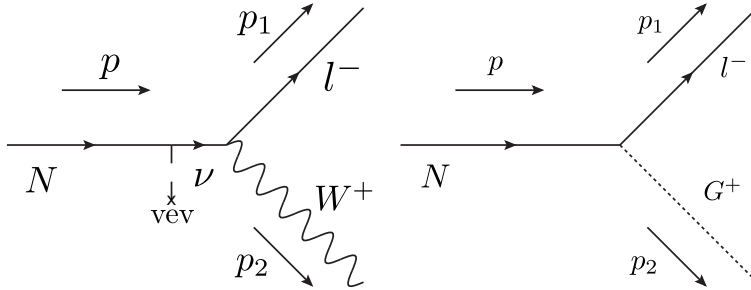


FIG. 1: $N \rightarrow W^+ l^-$ $1 \leftrightarrow 2$ channel. Since we have applied the Goldstone equivalence gauge, the Goldstone contribution is explicitly contained in the polarization vector, so we also need to calculate the Goldstone part of the diagrams.

The dispersion relations (or the “on-shell” equation) of the W/Z bosons below the critical temperature are complicated. Together with the dispersion relations of the leptons, and the conservation of energy and momentum equations, we have four equations to solve the phase space. Three of them are transcendental equations. Later we are going to describe the details to solve them.

In this paper, we rely on the Goldstone equivalent gauge[49] to calculate the sterile neutrino’s productions in the thermal plasma[45] below the critical temperature T_c . All the gauge polarizations and the Goldstone cadaver contributions are included. In the appendix, we will also show the equivalence between this gauge and the usually familiar R_ξ gauge.

In the following subsections we will describe the details for each channel. Before starting them, we also note that we ignore some of the sub-dominant tachyonic branch cuts in the bosonic propagators, as illustrated in our Ref. [45], and as in Ref. [23], the sub-dominant branch cuts in the leptonic propagators are also neglected.

A. W channels

The Feynmann diagram of a sterile neutrino N decaying into a W^+ boson and a charged lepton l^- is illustrated in Fig. 1. Since we are discussing a Dirac N , it is possible to inverse the arrows there to reformulate it into a \bar{N} decay diagram. We neglect the anti-sterile neutrino’s decay in our paper since the results are completely symmetric up to tree-level. The momentum flows are also defined in Fig. 1 and are defined relative to the plasma

background reference, i.e., the plasma's four-vector velocity

$$u^\mu = (1, 0, 0, 0). \quad (4)$$

When, e.g., $p_1^0 < 0$, the same diagram can also be interpreted as a charged lepton's fusion with the sterile neutrino to generate a W^+ boson, which is the dual process of a W^+ decaying into a N, l^+ pair. This is the ‘‘inverse-decay’’ process of a W^+ boson, we denote it with ‘‘ID’’ for abbreviation later. The thermal equilibrium condition guarantees the equality of the results from both the aspects of ‘‘decay’’ and ‘‘inverse-decay’’ processes of a W boson. Therefore, Fig. 1 can summarize all the possible $1 \leftrightarrow 2$ processes of a (anti-)sterile neutrino.

The dispersion relation of a W boson is given by

$$F_{W,(L,T)}(p_2) = p_2^2 - [m_W(T)]^2 - \Pi_{L,T}^W(p_2) = 0, \quad (5)$$

for transverse and longitudinal polarizations respectively, where

$$\begin{aligned} \Pi_L^W(p_2) &= -\frac{2m_{E2}^2 p_2^2}{\vec{p}_2^2} \left(1 - \frac{p_2^0}{|\vec{p}_2|} Q_0\left(\frac{p_2^0}{|\vec{p}_2|}\right) \right), \\ \Pi_T^W(p_2) &= \frac{1}{2}(2m_{E2}^2 - \Pi_L^W(p_2)), \end{aligned} \quad (6)$$

and

$$Q_0(x) = \frac{1}{2} \ln \frac{x+1}{x-1}. \quad (7)$$

The vev dependent W boson mass is given by

$$m_W(T) = \frac{g_2 v(T)}{2}, \quad (8)$$

where g_2 is the weak coupling constant, and the Debye thermal mass m_{E2} takes the form

$$m_{E2}^2 = \frac{11}{6} g_2^2 T^2. \quad (9)$$

Ignoring the lepton's vev dependent mass, since it is much smaller than the thermal mass term, the dispersion relation of the active lepton is given by (See page 140 in Ref. [50])

$$F_l(p_1) = [\Delta_+(p_1)\Delta_-(p_2)]^{-1} = 0, \quad (10)$$

where

$$\Delta_\pm(p_1) = \left(p_1^0 \mp |\vec{p}_1| - \frac{m_f^2}{2|\vec{p}_1|} \left[\left(1 \mp \frac{p_1^0}{|\vec{p}_1|} \right) \ln \frac{p_1^0 + |\vec{p}_1|}{p_1^0 - |\vec{p}_1|} \pm 2 \right] \right)^{-1}. \quad (11)$$

Here

$$m_f^2 = \frac{g_1^2 + 3g_2^2}{32} T^2. \quad (12)$$

The energy and momentum conservation laws are given by

$$p^0 = p_1^0 + p_2^0, \quad (13)$$

$$\vec{p}_2^2 = \vec{p}^2 + \vec{p}_1^2 - 2|\vec{p}||\vec{p}_1| \cos \theta_p, \quad (14)$$

where θ_p is the angle between \vec{p} and \vec{p}_1 . The subscript “ p ” denotes the “plasma”, which means that this is the angle measured in the plasma rest frame. Given the sterile neutrino’s energy and momentum p^0 , \vec{p} , fixing the θ_p , there are four unknown parameters p_1^0 , p_2^0 , $|\vec{p}_1|$, $|\vec{p}_2|$ in just four equations (5, 10, 13, 14). Solving these equations might give a set of solutions. If p_1^0 or p_2^0 is smaller than zero, it means that a lepton or a W boson becomes an initial particle. For the leptonic $p_1^2 > m_f^2$, this means a “particle” lepton participating the process, and when $p_1^2 < m_f^2$, this indicates a “hole”. We need to find all of the solutions to sum over all their contributions to the “interaction rate” γ_N .

With the acquired p_1 and p_2 , we can then calculate the amplitude. In the Goldstone equivalence gauge, the “polarization vector” of a gauge boson is extended to a five-component vector $\epsilon_{\pm, Lin}^{Wn}(p_2) = \epsilon_{\pm, Lout}^{Wn*}(p_2)$, $n = \mu, 4$ to include the Goldstone component ($n = 4$ denotes the Goldstone component). When contracting the indices, the $[g^{\mu\nu}] = \text{diag}[1, -1, -1, -1]$ is also extended to $[g^{mn}] = \text{diag}[1, -1, -1, -1, -1]$. The transverse polarization is the same as the R_ξ gauge with $\epsilon_{\pm}^{W4}(p_2) = \epsilon_{\pm}^{W0}(p_2) = 0$, and $\epsilon_{\pm}^{Wi}(p_2)p_{2i} = 0$. The longitudinal polarization $\epsilon_{Lin}^{Wn*}(p_2) = \epsilon_{Lout}^{Wn}(p_2)$ is given by

$$\epsilon_{Lout}^W(p_2) = \begin{pmatrix} -\frac{\sqrt{p_2^2}}{n_2 \cdot p_2} n_2^\mu \\ -i \frac{m_W(T)}{\sqrt{p_2^2}} \end{pmatrix}, \quad (15)$$

where $n_2^\mu = (1, -\frac{\vec{p}_2}{|\vec{p}_2|})$ for the convention of $(k^\mu) = (k^0, \vec{k})$ for any four-dimensional momentum k .

For the lepton spinors, we need to define

$$\tilde{p}_1 = p_1^0 (1, \pm \frac{\vec{p}_1}{|\vec{p}_1|}), \quad (16)$$

where for a “particle”, i.e., $p_1^2 > m_f^2$, the “+” sign is adopted, and for a “hole”, i.e., $p_1^2 < m_f^2$, the “-” sign is adopted. When $p_1^0 > 0$, a lepton (either a “particle” or a “hole”) is created and

a $\bar{u}^s(\tilde{p}_1)$ appears in the amplitude. When $p_1^0 < 0$, an anti-lepton (either an anti-“particle” or an anti-“hole”) is destroyed and a $\bar{v}^s(-\tilde{p}_1)$ appears in the amplitude respectively.

The amplitude of the gauge component, as denoted in the left panel of Fig. 1, then becomes

$$i\mathcal{M}_W^\mu = -y_N v(T) \frac{g_2}{\sqrt{2}} \bar{u}^s(\tilde{p}_1) \gamma^\mu P_L \frac{i}{\not{p}_{lT}} u^r(p), \quad (17)$$

when $p_1^0 > 0$ for the decay channel. If $p_1^0 < 0$, we only need to change the $\bar{u}^s(\tilde{p}_1)$ into $\bar{v}^s(-\tilde{p}_1)$ for the W -boson’s inverse-decay channel. The Goldstone component of the amplitude as denoted in the right panel of Fig. 1, is written to be

$$i\mathcal{M}_W^4 = -\sqrt{2} y_N \bar{u}^s(\tilde{p}_1) P_R u^r(p). \quad (18)$$

Again when $p_1^0 < 0$, $\bar{u}(\tilde{p}_1)$ needs to be replaced with $\bar{v}(-\tilde{p}_1)$. In the above equations, $P_{L,R} = \frac{1 \mp \gamma^5}{2}$, and the definition of p_{lT} is

$$p_{lT} = (p_{lT}^0, \vec{p}_{lT}) = \left(\left(1 - \frac{m_f^2 L}{p^0}\right) p^0, \left(1 + \frac{m_f^2 (1 - p^0 L)}{\vec{p}^2}\right) \vec{p} \right), \quad (19)$$

where

$$L = \frac{1}{2|\vec{p}|} \ln \frac{p^0 + |\vec{p}|}{p^0 - |\vec{p}|}. \quad (20)$$

The complete amplitude should take the form

$$\epsilon_{(t)n}^W(p_2) (i\mathcal{M}_W^n), \quad (21)$$

where $n = 0, 1, 2, 3, 4$, $t = \pm, L, out$. The squared amplitude should also take the statistic factor and the “renormalization constant”. The complete result is

$$A_{W,t} = \sum_{r,s=1,2} \mathcal{M}_W^n \mathcal{M}_W^{*m} \epsilon_{tn}^W \epsilon_{tm}^{W*} f_F\left(\frac{p_1^0}{T}\right) f_B\left(\frac{p_2^0}{T}\right) Z_l(p_1) Z_{Wt}(p_2), \quad (22)$$

where $t = \pm, L$ indices are not summed by the Einstein’s sum rule, and

$$f_F(x) = \frac{e^x}{e^x + 1}, \quad (23)$$

$$f_B(x) = \left| \frac{e^x}{e^x - 1} \right|, \quad (24)$$

and the “renormalization factors” are

$$Z_{W(T,L)}(p_2) = \frac{2p_2^0}{2p_2^0 - \frac{\partial \Pi_{T,L}^W(p_2)}{\partial p_2^0}}, \quad (25)$$

$$Z_l(p_1) = \frac{(p_1^0)^2 - \vec{p}_1^2}{2m_f^2}. \quad (26)$$

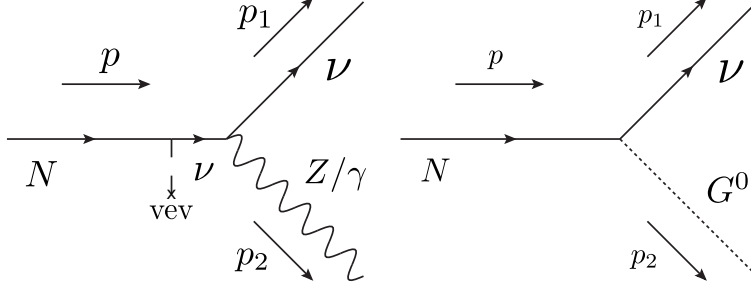


FIG. 2: $N \rightarrow (Z/\gamma)\nu$ 1 \leftrightarrow 2 channel.

B. Z/γ channels

Since W and B bosons receive the different thermal corrections, it disturbs the mixing angle for the “on-shell” Z/γ bosons. The mixing angles of the on-shell Z/γ bosons depend on their energy and momentum, so it is difficult to identify which is the Z or γ degree of freedom.

The vev dependent mass matrix for the B/W^3 field, or Z/γ particle is as usual

$$m_{Z/\gamma}^2(T) = \frac{(v(T))^2}{4} \begin{pmatrix} g_1^2 & -g_1 g_2 \\ -g_1 g_2 & g_2^2 \end{pmatrix}. \quad (27)$$

Thermal effects correct the B and W^3 mass terms respectively, therefore the thermal mass matrix is given by

$$\Pi_{T,L}^{Z/\gamma}(p_2) = \begin{pmatrix} \Pi_{T,L}^B(p_2) & 0 \\ 0 & \Pi_{T,L}^W(p_2) \end{pmatrix}, \quad (28)$$

where $\Pi_{T,L}^W(p_2)$ had already been given by (6). $\Pi_{T,L}^B$ changes the m_{E2} in (6) into m_{E1} ,

$$m_{E1}^2 = \frac{11}{6} g_1^2 T^2. \quad (29)$$

The dispersion rate of this mixed Z/γ is given by the “secular equation”

$$F_{Z/\gamma,(T,L)}(p_2) = \det(p_2^2 I_{2 \times 2} - m_{Z/\gamma}^2(T) - \Pi_{T,L}^{Z/\gamma}(p_2)) = 0, \quad (30)$$

for a transverse/longitudinal Z/γ vector boson. $I_{2 \times 2}$ is the 2×2 identical matrix. For a given p_2 as a solution of (30), matrix $p_2^2 I_{2 \times 2} - m_{Z/\gamma}^2(T) - \Pi_{T,L}^{Z/\gamma}(p_2)$ has a zero eigenvalue, and the corresponding eigenvector is denoted by $x = \begin{pmatrix} x_1 \\ x_2 \end{pmatrix}$, where $x_1^2 + x_2^2 = 1$. In the zero

temperature case, $x_1^Z = -\sin\theta_W$, $x_2^Z = \cos\theta_W$ for Z boson, and $x_1^\gamma = \cos\theta_W$, $x_2^\gamma = \sin\theta_W$ for the photon, where θ_W is the Weinberg angle. Since the neutrino does not interact with a pure photon, we can calculate the inner product $x \cdot x^Z = -x_1 \sin\theta_W + x_2 \cos\theta_W$ to extract the Z part of the “on-shell” mixed boson to calculate its interactions with the leptons. The dispersion relation of a lepton and the energy-momentum conservation law is exactly the same with (10, 13, 14) in Sec. II A. Solve these equations with (30), we then acquire all the “on-shell” p_1 and p_2 .

The transverse polarization vectors of a Z/γ boson $\epsilon_\pm^{Z/\gamma n}$ is the same as the W-boson $\epsilon_\pm^{W n}$ to satisfy $p_{2\mu}\epsilon_\pm^{Z/\gamma\nu} = 0$, $\epsilon_\pm^{Z/\gamma 4} = 0$ and $p_{2i}\epsilon_\pm^{Z/\gamma i} = 0$. The longitudinal polarization vector is given by

$$\epsilon_{Lin}^{Z/\gamma*}(p_2) = \epsilon_{Lout}^{Z/\gamma}(p_2) = \begin{pmatrix} -\frac{\sqrt{p_2^0}}{n_2 \cdot p_2} n_2^\mu \\ -i\frac{m_Z(T)}{\sqrt{p_2^0}}(-x_1 \sin\theta_W + x_2 \cos\theta_W) \end{pmatrix}. \quad (31)$$

Compared with the (15), the extra $(-x_1 \sin\theta_W + x_2 \cos\theta_W)$ factor in the Goldstone component indicates that only the Z -component of the vector boson had “eaten” some Goldstone boson. The photon part of this vector boson had not devoured any Goldstone fraction.

Then we are ready to write the amplitudes.

$$i\mathcal{M}_{Z/\gamma}^\mu = -y_N v(T) \frac{g_2}{2 \cos\theta_W} \bar{u}^s(\tilde{p}_1) \gamma^\mu P_L \frac{i}{\not{p}_{lT}} u^r(p) (-x_1 \sin\theta_W + x_2 \cos\theta_W), \quad (32)$$

$$i\mathcal{M}_{Z/\gamma}^4 = -y_N \bar{u}^s(\tilde{p}_1) P_R u^r(p). \quad (33)$$

The total result of the squared amplitude is

$$A_{Z/\gamma,t} = \sum_{r,s=1,2} \mathcal{M}_{Z/\gamma}^n \mathcal{M}_{Z/\gamma}^{*m} \epsilon_{tn}^{Z/\gamma} \epsilon_{tm}^{Z/\gamma*} f_F\left(\frac{p_1^0}{T}\right) f_B\left(\frac{p_2^0}{T}\right) Z_l(p_1) Z_{Z/\gamma t}(p_2), \quad (34)$$

where the “renormalization constant” $Z_{Z/\gamma(T/Lout)}(p_2)$ is calculated to be

$$Z_{Z/\gamma(T,L)}(p_2) = \frac{2p_2^0}{2p_2^0 - \Pi_{(T,L),p_2^0}^{Z/\gamma, \text{ on shell}}(p_2)}, \quad (35)$$

and $\Pi_{(T,L),p_2^0}^{Z/\gamma, \text{ on shell}}(p_2) = x^T \frac{\partial \Pi_{T,L}^{Z/\gamma}(p_2)}{\partial p_2^0} x$ so that

$$\Pi_{T,L}^{Z/\gamma, \text{ on shell}}(p_2) = x_1^2 \frac{\partial \Pi_{T,L}^B(p_2)}{\partial p_2^0} + x_2^2 \frac{\partial \Pi_{T,L}^W(p_2)}{\partial p_2^0}. \quad (36)$$

C. Goldstone channels

Besides the Goldstone component in the Z_L and W_L polarization vectors, the Goldstone cadavers also contribute to the $1 \leftrightarrow 2$ rate. Rigorously speaking these remains are no longer a “particle” since they are “branch cuts” rather than “poles”. However, since the imaginary parts peak significantly at $p_2^0 = \pm|\vec{p}_2|$, we could apply the approximation to regard them as massless bosons. The corresponding Feynmann diagrams are the same as the second panels in Fig. 1, 2 with the only difference that the Goldstone cadavers are no longer bounded with the longitudinal polarizations of the W and Z bosons.

The dispersion relation of a “massless” Goldstone boson is simple,

$$F_G(p_2) = (p_2^0)^2 - \vec{p}_2^2 = 0. \quad (37)$$

Other equations are the same as the previous subsections. After solving (10, 13, 14) with (37), we then write down the final result of the squared amplitude

$$A_{G^\pm} = \sum_{r,s=1,2} \mathcal{M}_W^4 \mathcal{M}_W^{*4} f_F\left(\frac{p_1^0}{T}\right) f_B\left(\frac{p_2^0}{T}\right) Z_l(p_1) Z_{G^\pm}(p_2) \quad (38)$$

for the charged Goldstone channel, where $Z_{G^0}(p_2)$ is calculated and defined by

$$Z_{G^\pm}(p_2) = \frac{2|\vec{p}_2|}{\pi} \int_0^{|\vec{k}|+\delta} \text{Im}\left[i \frac{p_2^2 - \Pi_L^W(p_2) + i\epsilon}{p_2^2 - [m_W(T)]^2 - \Pi_L^W(p_2) + i\epsilon} \frac{i}{p_2^2 + i\epsilon}\right] dk^0, \quad (39)$$

and the final result

$$A_{G^0} = \sum_{r,s=1,2} \mathcal{M}_{Z/\gamma}^4 \mathcal{M}_{Z/\gamma}^{*4} f_F\left(\frac{p_1^0}{T}\right) f_B\left(\frac{p_2^0}{T}\right) Z_l(p_1) Z_{G^0}(p_2) \quad (40)$$

for the neutral Goldstone channel, where

$$Z_{G^0}(p_2) = \frac{2|\vec{p}_2|}{\pi} \int_0^{|\vec{k}|+\delta} \text{Im}\left[i \frac{(p_2^2 - \Pi_L^{11} + i\epsilon)(p_2^2 - \Pi_L^{22} + i\epsilon) - (\Pi_L^{12})^2}{(p_2^2 - [m_Z(T)]^2 - \Pi_L^{11} + i\epsilon)(p_2^2 - \Pi_L^{22} + i\epsilon) - (\Pi_L^{12})^2} \frac{i}{p_2^2 + i\epsilon}\right] dk^0. \quad (41)$$

Here $m_Z(T) = \frac{\sqrt{g_1^2 + g_2^2}}{2} v(T)$, and

$$\begin{aligned} \Pi_L^{11} &= \Pi_L^B \sin^2 \theta_W + \Pi_L^W \cos^2 \theta_W, \\ \Pi_L^{22} &= \Pi_L^B \cos^2 \theta_W + \Pi_L^W \sin^2 \theta_W, \\ \Pi_L^{12} &= \Pi_L^W \cos \theta_W \sin \theta_W - \Pi_L^B \cos \theta_W \sin \theta_W. \end{aligned} \quad (42)$$

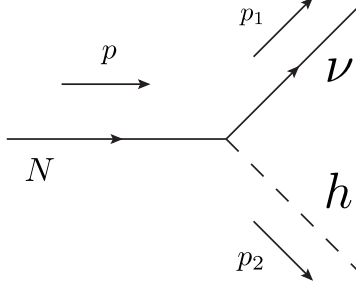


FIG. 3: $N \rightarrow h\nu$ $1 \leftrightarrow 2$ channel.

D. Higgs channels

The Higgs channel is quite straightforward, since the Higgs boson only receives a trivial mass correction from the thermal environment. Below the T_c , the $m_h(T) \propto v(T)$, so

$$m_h(T) = m_{h0} \sqrt{1 - \frac{T^2}{T_c^2}}, \quad (43)$$

and above the T_c , $m_h(T)$ becomes

$$m_h^2(T) = (g_1^2 + 3g_2^2 + 4y_t^2 + 8\lambda) \frac{T^2 - T_c^2}{16}, \quad (44)$$

where $m_{h0} = 125$ GeV. Therefore the dispersion relation of a Higgs boson is simply

$$F_H(p_2) = p_2^2 - m_h(T)^2 = 0. \quad (45)$$

Again solving (10, 13, 14) with (45) for the valid p_1 and p_2 , we then write down the amplitude,

$$i\mathcal{M}_h = iy_N \bar{u}^s(\tilde{p}_1) P_R u^r(p). \quad (46)$$

The total result of the squared amplitude is

$$A_h = \sum_{r,s=1,2} \mathcal{M}_h \mathcal{M}_h^* f_F\left(\frac{p_1^0}{T}\right) f_B\left(\frac{p_2^0}{T}\right) Z_l(p_1). \quad (47)$$

III. PHASE SPACE AND THERMAL AVERAGE INTEGRATION

In the thermal background, the Lorentz invariance had been broken so that we could not directly “boost” the center of momentum reference frame to calculate the $1 \leftrightarrow 2$ processes

of a sterile neutrino at rest. We could only rely on the definition of a width at any reference frame

$$\begin{aligned}
\Gamma_X &= \frac{1}{2p^0} \int \frac{d^3\vec{p}_1 d^3\vec{p}_2}{(2\pi)^6} \frac{A_X}{(2p_1^0)(2p_2^0)} (2\pi)^4 \delta^4(p - p_1 - p_2) \\
&= \frac{1}{2p^0} \int \frac{d^3\vec{p}_1}{(2\pi)^6} \frac{A_X}{(2p_1^0)(2p_2^0)} (2\pi)^4 \delta(p^0 - p_1^0 - p_2^0) \\
&= \frac{1}{2p^0} \int \frac{2\pi \sin \theta_p \vec{p}_1^2 d|\vec{p}_1| d\theta_p}{(2\pi)^6} \frac{A_X}{(2p_1^0)(2p_2^0)} (2\pi)^4 \delta(p^0 - p_1^0 - p_2^0)
\end{aligned} \tag{48}$$

where $X = [W, (T, \text{Lout})], [Z/\gamma, (T, \text{Lout})], G^\pm, G^0, h$, and we also applied the symmetry of the system rotating along the \vec{p} axis, thus eliminating the ϕ angle to be 2π . To integrate out the δ function, we calculate

$$\frac{\partial p_1^0}{\partial |\vec{p}_1|} + \frac{\partial p_2^0}{\partial |\vec{p}_1|} = \frac{\partial p_1^0}{\partial |\vec{p}_1|} + \frac{\partial p_2^0}{\partial |\vec{p}_2|} \frac{\partial |\vec{p}_2|}{\partial |\vec{p}_1|}. \tag{49}$$

$\frac{\partial |\vec{p}_2|}{\partial |\vec{p}_1|}$ is extracted from the momentum conservation law (14), the result is

$$\frac{\partial |\vec{p}_2|}{\partial |\vec{p}_1|} = \frac{|\vec{p}_1| - |\vec{p}| \cos \theta_p}{|\vec{p}_2|}. \tag{50}$$

$\frac{\partial p_1^0}{\partial |\vec{p}_1|}$ and $\frac{\partial p_2^0}{\partial |\vec{p}_2|}$ can be extracted from the corresponding dispersion relations (5, 30, 37, 45). Generally, if the dispersion relation of a momentum p_Y is written to be $F_X(p_Y) = F_X(p_Y^0, |\vec{p}_Y|) = 0$, where $X = l, [W, (T, \text{Lout})], [Z/\gamma, (T, \text{Lout})], G, H$, then

$$\frac{\partial p_Y^0}{\partial |\vec{p}_Y|} = - \frac{\frac{\partial F_X(p_Y)}{\partial |\vec{p}_Y|}}{\frac{\partial F_X(p_Y)}{\partial p_Y^0}}. \tag{51}$$

Therefore, (49) can be reduced to

$$\Gamma_X = \frac{1}{2p^0} \int \frac{2\pi \sin \theta_p \vec{p}_1^2 d\theta_p}{(2\pi)^6} \frac{A_X}{(2p_1^0)(2p_2^0)} \frac{(2\pi)^4}{\left| \frac{\frac{\partial F_X(p_1)}{\partial |\vec{p}_1|}}{\frac{\partial F_X(p_1)}{\partial p_1^0}} + \frac{\frac{\partial F_X(p_2)}{\partial |\vec{p}_2|}}{\frac{\partial F_X(p_2)}{\partial p_2^0}} \frac{|\vec{p}_1| - |\vec{p}| \cos \theta_p}{|\vec{p}_2|} \right|}. \tag{52}$$

Straightforwardly applying (52) also takes a problem. For each θ_p , sometimes there are multiple solutions for $p_1^0, \vec{p}_1, p_2^0, \vec{p}_2$. This is because when the sterile neutrino decays to every direction in its center of momentum frame, however, boosted to the plasma reference frame, one angle can pick up two different momentum. To correctly picking up all the possibilities, we still need to calculate the phase space in the sterile neutrino's rest frame by boosting the p_1, p_2 into p_{1N}, p_{2N} . We then use $p_{1,2N}$ as the input parameters to solve the various

dispersion relations. Take the x-axis along the \vec{p} direction, and without loss of generality, let \vec{p}_1 be located in the x-y plain, we have

$$p_{1N}^0 = \gamma(p_1^0 - \beta|\vec{p}_1| \cos \theta_p), \quad (53)$$

$$|\vec{p}_{1N}| \cos \theta_N = \gamma(|\vec{p}_1| \cos \theta_p - \beta p_1^0), \quad (54)$$

$$|\vec{p}_{1N}| \sin \theta_N = |\vec{p}_1| \sin \theta_p, \quad (55)$$

where $\beta = \frac{|\vec{p}|}{p^0}$, $\gamma = \frac{1}{\sqrt{1-\beta^2}}$. A tedious calculation finally shows that

$$\frac{d\theta_N}{d\theta_p} = \frac{\partial\theta_N}{\partial\theta_p} + \frac{\partial\theta_N}{\partial p_1^0} \frac{\partial p_1^0}{\partial\theta_p} + \frac{\partial\theta_N}{\partial|\vec{p}_1|} \frac{\partial|\vec{p}_1|}{\partial\theta_p}, \quad (56)$$

where

$$\frac{\partial\theta_N}{\partial\theta_p} = \frac{\vec{p}_1^2 \gamma (-|\vec{p}_1| + p_1^0 \beta \cos \theta_p) \sin \theta_p}{[\gamma^2 (p_1^0 \beta - |\vec{p}_1| \cos \theta_p)^2 + \vec{p}_1^2 \sin^2 \theta_p]^{\frac{3}{2}}} \frac{1}{(-\sin \theta_N)}, \quad (57)$$

$$\frac{\partial\theta_N}{\partial p_1^0} = \frac{-\vec{p}_1^2 \beta \gamma \sin^2 \theta_p}{[\gamma^2 (p_1^0 \beta - |\vec{p}_1| \cos \theta_p)^2 + \vec{p}_1^2 \sin^2 \theta_p]^{\frac{3}{2}}} \frac{1}{(-\sin \theta_N)}, \quad (58)$$

$$\frac{\partial\theta_N}{\partial|\vec{p}_1|} = \frac{p_1^0 |\vec{p}_1| \beta \gamma \sin^2 \theta_p}{[\gamma^2 (p_1^0 \beta - |\vec{p}_1| \cos \theta_p)^2 + \vec{p}_1^2 \sin^2 \theta_p]^{\frac{3}{2}}} \frac{1}{(-\sin \theta_N)}, \quad (59)$$

$$\frac{\partial p_1^0}{\partial\theta_p} = \frac{|\vec{p}| |\vec{p}_1| \sin \theta_p}{-\frac{\partial|\vec{p}_1|}{\partial p_1^0} |\vec{p}_1| - \frac{\partial|\vec{p}_2|}{\partial p_2^0} |\vec{p}_2| + \frac{\partial|\vec{p}_1|}{\partial p_1^0} |\vec{p}| \cos \theta_p}, \quad (60)$$

$$\frac{\partial|\vec{p}_1|}{\partial\theta_p} = \frac{|\vec{p}| |\vec{p}_1| \sin \theta_p}{-\vec{p}_1 - \frac{\partial\vec{p}_2}{\partial p_2^0} \frac{\partial p_1^0}{\partial|\vec{p}_1|} |\vec{p}_2| + |\vec{p}| \cos \theta_p}, \quad (61)$$

and the $\frac{\partial|\vec{p}_i|}{\partial p_i^0}$ had been already calculated in (51). Then we can replace the $d\theta_p$ with $d\theta_N \frac{d\theta_p}{d\theta_N}$ in (52) to calculate this integration.

The thermal average integration is simple,

$$\gamma_X = \int \frac{d^3\vec{p}}{(2\pi)^3} e^{-\frac{p^0}{T}} \Gamma_X, \quad (62)$$

where g_N is the degree of freedom. This γ_X will enter the Boltzmann equation.

Let us summarize the numerical algorithm processes. To calculate one channel, e.g., $N \leftrightarrow Wl$ or $Nl \leftrightarrow W$, one needs to follow these steps:

- Fix the p^0 , \vec{p} , and θ_N , we are going to solve the p_{1N}^0 , p_{2N}^0 , \vec{p}_{1N} , \vec{p}_{2N} . The equations to be solved are (5, 10, 13, 14). They are defined with the parameters p_1^0 , p_2^0 , \vec{p}_1 , \vec{p}_2 and θ_p , and these two sets of parameters are mediated by the (53-55).

Alias	Meaning	Alias	Meaning
WTD	$N \leftrightarrow W_T^+ l^-$	Z γ LID	$N\bar{\nu} \leftrightarrow Z_L/\gamma_L$
WTID	$Nl^+ \leftrightarrow W_T^+$	G^\pm D	$N \leftrightarrow G^+ l^-$
WLD	$N \leftrightarrow W_L^+ l^-$	G^\pm ID	$NG^- \leftrightarrow l^-, Nl^+ \leftrightarrow G^+$
WLID	$Nl^+ \leftrightarrow W_L^+$	G^0 D	$NG^0 \leftrightarrow \nu, N\bar{\nu} \leftrightarrow G^0$
Z γ TD	$N \leftrightarrow Z_T/\gamma_T \nu$	G^0 ID	$NG^0 \leftrightarrow \nu, N\bar{\nu} \leftrightarrow G^0$
Z γ TID	$N\bar{\nu} \leftrightarrow Z_T/\gamma_T$	HD	$N \leftrightarrow h\nu$
Z γ LD	$N \leftrightarrow Z_L/\gamma_L \nu$	HID	$Nh \leftrightarrow \nu, N\bar{\nu} \leftrightarrow h$

TABLE I: Channels to be plotted and their meanings.

- With the acquired numerical solution of p_1 , p_2 and θ_p , calculate the total squared amplitude through (22).
- Changing θ_N , utilize (52, 56) to compute the $\Gamma_{W,T/L}$.
- Change p to calculate (62).

IV. NUMERICAL RESULTS

We have scanned the $m_N \in [50, 200]$ GeV range by an interval of 1 GeV. For the leptonic sector, both “particle” and “hole” channels had been included. For the bosonic sector, all the transverse, longitudinal vector boson, and the Goldstone, Higgs channels had been considered. We have enumerated all the $1 \leftrightarrow 2$ possibilities, however, it is unnecessary to plot all of them. We sum over the results into 14 channels, and show the meaning of them in Tab. I. Notice that the channel $N(W/Z) \leftrightarrow l^-/\nu$ had been kinematically forbidden in our interested parameter space, so that they had been neglected. Compared with the production rate γ_X , it is more convenient to use the averaged decay width

$$\bar{\Gamma}_X = \frac{\gamma_X}{n_N^{\text{eq}}} = \frac{\int \frac{d^3\vec{p}}{(2\pi)^3} e^{-\frac{p^0}{T}} \Gamma_X}{2 \frac{m_N^2 T}{2\pi^2} K_2\left(\frac{m_N}{T}\right)}, \quad (63)$$

since its comparison with the Hubble constant $H \simeq 1.66\sqrt{g_*} \frac{T^2}{M_{\text{pl}}}$ can help us judge whether the sterile neutrino start to deviate from the thermal equilibrium conveniently.

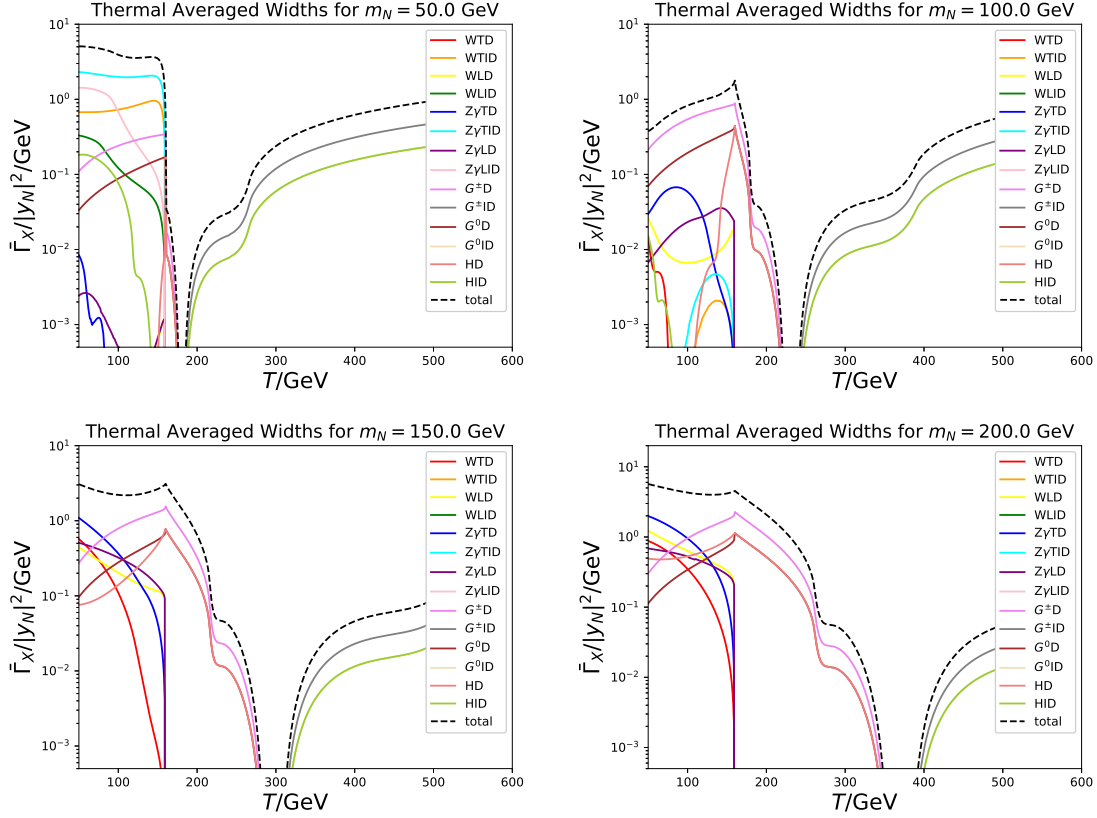


FIG. 4: Thermal averaged widths plot normalized by $\frac{1}{|y_N|^2}$ for $m_N = 50, 100, 150, 200$ GeV masses. The meanings in the legends are illustrated in Tab. I.

In Fig. 4, we have selected the $m_N = 50, 100, 150, 200$ GeV to plot their thermal averaged widths normalized by $\frac{1}{|y_N|^2}$ depending on the temperature T . Just below the critical temperature $100 \text{ GeV} \lesssim T < T_c$, the longitudinal W/Z and the Goldstones play the crucial roles. These two kinds of channels are complementary, and compared with the corresponding part of the Fig. 1 in Ref. [40], in which large areas had been kinematically forbidden within the $100 \text{ GeV} \lesssim T < T_c$, $50 \text{ GeV} \lesssim m_N \lesssim 100 \text{ GeV}$ ranges there, our calculations does not give such a remarkable suppression. To show this clearly, we also plot a total thermal averaged width $\bar{\Gamma}_{\text{tot}} = \sum_X \bar{\Gamma}_X$ in Fig. 5. There we can see a similar suppression of the total thermal averaged width when $T > T_c$ compared with the Fig. 1 in Ref. [40], while when $T < T_c$, only a slight and obscure suppression appears in roughly the same area.

In the rest of this section we show a preliminary calculation of the leptogenesis with all the results above. Above the sphaleron decoupling temperature when $T > T_{\text{sph}} = 131.7$

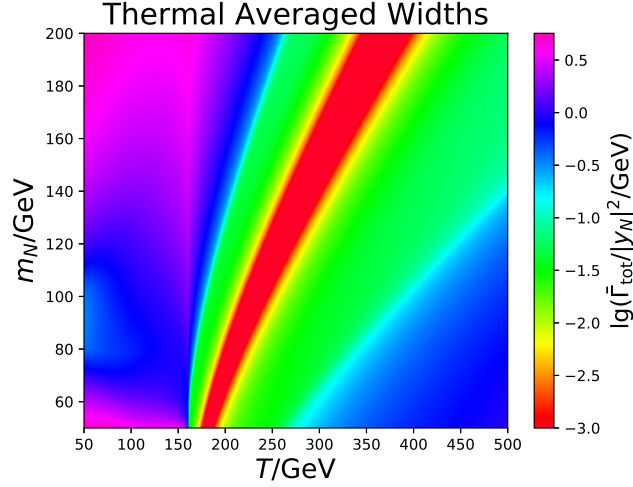


FIG. 5: Total $\bar{\Gamma}_{\text{tot}} = \sum_X \bar{\Gamma}_X$ normalized by $\frac{1}{|y_N|^2}$ depending on the temperature T and the sterile neutrino mass m_N . To keep the image contrast in the other area where the $1 \leftrightarrow 2$ processes are not suppressed kinematically, we just keep $\frac{\bar{\Gamma}_{\text{tot}}}{|y_N|^2} \geq 1.0 \times 10^{-3}$ GeV in this image. Therefore, most of the red parts in this image are actually much smaller than those plotted here.

GeV[51], the $B + L$ number does not conserve, so the lepton number asymmetry generated from the sterile neutrino $1 \leftrightarrow 2$ processes is ported to the baryon number asymmetry through the sphaleron effects. To explain the observed ratio of baryon asymmetry normalized by the photon number density $|\eta_{B0}| = \frac{|n_B - n_{\bar{B}}|}{n_\gamma} \approx 6 \times 10^{-10}$ in our current universe, $|\eta^L| = \frac{|n_L - n_{\bar{L}}|}{n_\gamma}$ is calculated then to be 2.47×10^{-8} [37] at $T = T_{\text{sph}} = 131.7$ GeV. Including the $2 \leftrightarrow 2$ wash-out terms, the Boltzmann equations are given by

$$\begin{aligned} \frac{n_\gamma H_N}{z} \frac{d\eta_N}{dz} &= \left(1 - \frac{\eta_N}{\eta_N^{\text{eq}}}\right) [\gamma_D + 2(\gamma_{Hs} + \gamma_{As}) + 4(\gamma_{Ht} + \gamma_{At})], \\ \frac{n_\gamma H_N}{z} \frac{d\eta_L}{dz} &= \gamma_D \left[\left(\frac{\eta_N}{\eta_N^{\text{eq}}} - 1\right) \epsilon_{\text{CP}}(z) - \frac{2}{3}\eta_L \right] - \frac{4}{3}\eta_L \left[2(\gamma_{Ht} + \gamma_{At}) + \frac{\eta^N}{\eta_{\text{eq}}^N}(\gamma_{Hs} + \gamma_{As}) \right] \end{aligned} \quad (64)$$

where $\eta_N = \frac{n_N}{n_\gamma}$, $\gamma_D = \sum_X \gamma_X$ is the summation over all the $1 \leftrightarrow 2$ channels defined in (62). We shall neglect the $2 \leftrightarrow 2$ contributions $\gamma_{Hs, Ht, As, At}$ in this paper, since we only calculate the situation that the sterile neutrino is initially in thermal equilibrium with the plasma when $T \gg m_N$. When $T \sim m_N$ or $T \lesssim m_N$ that the deviation from the thermal equilibrium becomes significant, the $2 \leftrightarrow 2$ processes are usually suppressed by an additional $n_{A,H,\dots}^{\text{eq}}$ factor compared with the γ_D . The CP-source parameter $\epsilon_{\text{CP}}(z)$ originate from the one-loop interference with the tree-level results[32, 36], and should depend on z . The identification of

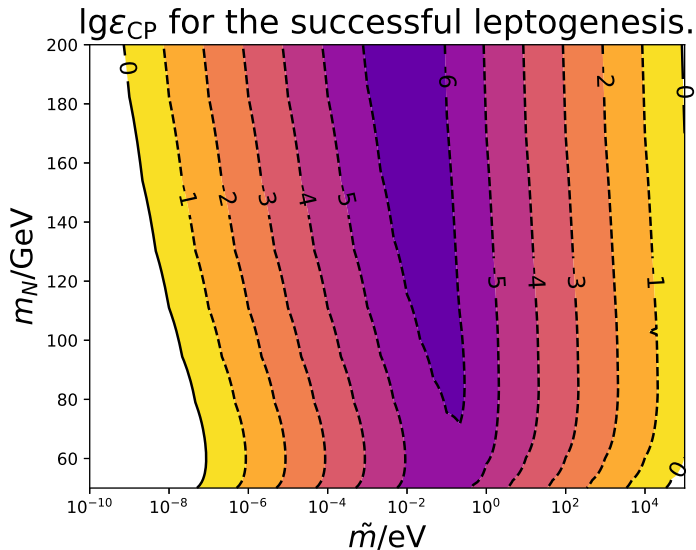


FIG. 6: $\lg \epsilon_{\text{CP}}$ needed to obtain the successful leptogenesis. The sterile neutrinos are initially in thermal equilibrium with the plasma.

this parameter is beyond the scope of this paper. We only follow the section II of Ref. [40] to regard ϵ_{CP} as a constant parameter to present our results of the successful leptogenesis in Fig. 6. At some proposed future leptonic colliders, with the aid of the secondary vertex detection, the sensitivity of y_N at ILC[52–56], CEPC[57, 58] and FCC-ee[59] can be significantly improved. Ref. [60–64] have discussed the search of such sterile neutrino at these colliders, and their results can roughly verify the parameter space $50 \text{ GeV} < m_N < 90 \text{ GeV}$ and $\tilde{m} \gtrsim 1 \text{ eV}$. Our contours had been significantly modified compared with the Fig. 3 in Ref. [40], especially for the $1 \text{ eV} \lesssim \tilde{m} \lesssim 10^5 \text{ eV}$ and $40 \text{ GeV} \lesssim m_N \lesssim 110 \text{ GeV}$ area there, where quite a large void appeared due to the absence of the γ_D kinematically forbidden below T_c in their Fig. 1. In our paper, such an area is filled up with the $N \leftrightarrow G^{+,0}(l^-/\nu)$, $N \leftrightarrow W_{T,L}^+ l^-$ or $N \leftrightarrow Z_{T,L} \nu$ channels, so that no significant distortions of the contours had been carried out.

V. SUMMARY

We have calculated the $1 \leftrightarrow 2$ processes of a sterile neutrino interacting with the gauge/Higgs bosons and leptons in the thermal plasma. We applied the Goldstone-equivalence gauge to evaluate the processes below the critical temperature $T_c \approx 160 \text{ GeV}$,

and our method is suitable for the sterile neutrino's mass $m_N \sim T_c$. The results can be utilized in the studies involving the sterile neutrinos, and we have calculated the preliminary leptogenesis as an example. Compared with the Ref. [40], the results had been significantly changed due to the different kinematic threshold understandings in this paper. $1 \leftrightarrow 2$ results are usually sufficient to study the processes in the temperature that is roughly of the same magnitude with the sterile neutrino's mass if one assumes an initially thermal equilibrium. Yet the Non-perturbative corrections that the leptons and bosons interchange soft particles with the plasma and with each other had not been included. To carry forward our research to a wider temperature scale and to a more precise calculation, we will include all these effects in our further studies.

Appendix A: Aspect from the R_ξ gauge

The equivalence of the R_ξ gauge and the Goldstone equivalent gauge is guaranteed by the Ward-Takahashi identity in the broken phase[65], where $p_2^\mu \mathcal{M}_{V\mu} = im_V \mathcal{M}^{\text{GS}}$, $V = Z/W$. For the W boson,

$$\epsilon_{L,R\xi}^W = \epsilon_{L\text{in}}^W + \begin{pmatrix} \frac{p_2^\mu}{\sqrt{p_2^2}} \\ -i \frac{m_W(T)}{\sqrt{p_2^2}} \end{pmatrix}, \quad (\text{A1})$$

One finds out that $\epsilon_{L,R\xi}^W$ is actually the usual longitudinal polarization vector which is the most widely applied, which does not change the amplitude according to the Ward-Takahashi identity in the broken phase. Due to the mixing between Z and γ vector bosons, the Z/γ polarizations are a little bit complicated. Notice that in the definition of (31), we are actually attributing the mixing parameter $-x_1 \sin \theta_W + x_2 \cos \theta_W$ appearing in the Goldstone couplings in the polarization vector, while leaving this parameter corresponding to the vector components in the coupling constants. Remember also for a pure γ , when p_2^μ dot into an amplitude will completely disappear. Therefore, if we define

$$\epsilon_{L,R\xi}^{Z/\gamma} = \epsilon_{L\text{in}}^{Z/\gamma} + \begin{pmatrix} \frac{p_2^\mu}{\sqrt{p_2^2}} \\ -i(-x_1 \sin \theta_W + x_2 \cos \theta_W) \frac{m_Z(T)}{\sqrt{p_2^2}} \end{pmatrix}, \quad (\text{A2})$$

we recover the most widely used $\epsilon_{L,R\xi}^{Z/\gamma}$ again which does not change the final results.

For the Goldstone channels, one can also replace the Goldstone external leg by a “vector boson” with the polarization vector $\frac{p_2^\mu}{im_V}$, equivalent to picking up the “quasi-poles” corresponding to the $\propto p_2^\mu p_2^\nu$ terms in the R_ξ propagator.

One might notice that the Ward-Takahashi identity is not rigorously satisfied if one tries to verify this identity on the practical formulas defined in (17, 18, 32, 33). However, if we include the hard thermal one-loop corrections to the gauge vertices (Page 161 in Ref. [50]),

$$\Gamma_\mu(p, p_1) = -m_f^2 \int \frac{d\Omega_{\hat{k}}}{4\pi} \frac{\hat{k}_\mu \hat{k}}{(p \cdot \hat{k})(p_1 \cdot \hat{k})}, \quad (\text{A3})$$

where m_f is again given by (12) and $\hat{k} = (1, \vec{k})$ and $\hat{k} \cdot \hat{k} = 1$, the Ward-Takahashi identity can be precisely satisfied perturbatively. This can be seen by dotting $p_2 = p - p_1$ into Γ_μ ,

$$(p - p_1) \cdot \Gamma(p, p_1) = -m_f^2 \int \frac{d\Omega_{\hat{k}}}{4\pi} \left[\frac{\hat{k}}{p_1 \cdot \hat{k}} - \frac{\hat{k}}{p \cdot \hat{k}} \right] = \Sigma(p) - \Sigma(p_1), \quad (\text{A4})$$

where $\Sigma(p)$ is the hard thermal one loop correction on a fermionic propagator of the active neutrino or a charged lepton. These two Σ 's will help cancel the denominator in the $\frac{i}{\not{p}_{(1)} - \Sigma(p_{(1)})}$ propagators on both sides of the gauge vertex, thus proving the Ward-Takahashi identity in the broken phase perturbatively.

Through a power-counting consideration, neglecting the (A3) will introduce a relative error of $\sim \frac{m_f^2}{m_N^2}$ in the final results. $\frac{m_f^2}{m_N^2} \lesssim 1$ induces $m_N \lesssim 0.15T$. Since the $W/Z/\gamma$ channels open up at $T < T_c$, and $0.15T_c = 24$ GeV, our interested range $m_N > 50$ GeV is sufficiently safe that (A3) can be neglected.

The Goldstone equivalence gauge applied in this paper also takes another advantage. If we fix on the R_ξ gauge, one might introduce a discontinuity of the total effective decay rate over the cross-over temperature T_c up to tree-level. Notice that below the T_c , the Goldstone cadaver contributions are collected within the $p_2^\mu p_2^\nu$ terms in the gauge boson components, while when $T > T_c$, all the Goldstone contributions originate from the Yukawa couplings. A smooth transition between these two coupling formalisms requires (A3), and neglecting this will introduce a discontinuity. Therefore, we can see that attributing all the “Goldstone contribution” of a vector boson to the Goldstone Yukawa couplings, just as what we did in the Goldstone equivalence gauge, will automatically include the (A3) corrections in the longitudinal-Goldstone involving terms. Therefore, at least for these terms other than the transverse polarization contributions, Goldstone equivalence gauge includes more hard thermal loop corrections on vertices for the longitudinal-Goldstone degrees of freedom.

Acknowledgments

We thank for Junmou Chen, Pyungwon Ko, Ligong Bian, Fa-Peng Huang, Chun Liu, Chen Zhang, Ye-Ling Zhou, Mikko Laine, Kechen Wang for helpful discussions and communications. This work is supported in part by the National Natural Science Foundation of China under Grants No. 11805288 and No. 11875327, the Natural Science Foundation of Guangdong Province under Grant No. 2016A030313313, the Fundamental Research Funds for the Central Universities, and the Sun Yat-Sen University Science Foundation.

-
- [1] M. Fukugita and T. Yanagida, Phys. Lett. B **174**, 45 (1986).
- [2] M. Luty, Phys. Rev. D **45**, 455 (1992).
- [3] T. Gherghetta and G. Jungman, Phys. Rev. D **48**, 1546 (1993), hep-ph/9302212.
- [4] M. Plumacher, Z. Phys. C **74**, 549 (1997), hep-ph/9604229.
- [5] M. Plumacher, Nucl. Phys. B **530**, 207 (1998), hep-ph/9704231.
- [6] W. Buchmuller and M. Plumacher, Phys. Lett. B **389**, 73 (1996), hep-ph/9608308.
- [7] W. Buchmuller and M. Plumacher, Phys. Rept. **320**, 329 (1999), hep-ph/9904310.
- [8] W. Buchmuller and M. Plumacher, Int. J. Mod. Phys. A **15**, 5047 (2000), hep-ph/0007176.
- [9] W. Buchmuller, P. Di Bari, and M. Plumacher, Annals Phys. **315**, 305 (2005), hep-ph/0401240.
- [10] S. Davidson, E. Nardi, and Y. Nir, Phys. Rept. **466**, 105 (2008), 0802.2962.
- [11] Y.-L. Tang and S.-h. Zhu (2015), [JHEP03,043(2016)], 1512.02899.
- [12] Y.-L. Tang and S.-h. Zhu, JHEP **01**, 025 (2017), 1609.07841.
- [13] B. Batell, T. Han, and B. Shams Es Haghi, Phys. Rev. **D97**, 095020 (2018), 1704.08708.
- [14] B. Batell, T. Han, D. McKeen, and B. Shams Es Haghi, Phys. Rev. **D97**, 075016 (2018), 1709.07001.
- [15] M. Escudero, N. Rius, and V. Sanz, Eur. Phys. J. **C77**, 397 (2017), 1607.02373.
- [16] R. Allahverdi, Y. Gao, B. Knockel, and S. Shalgar, Phys. Rev. **D95**, 075001 (2017), 1612.03110.
- [17] P. Bandyopadhyay, E. J. Chun, R. Mandal, and F. S. Queiroz, Phys. Lett. **B788**, 530 (2019), 1807.05122.
- [18] P. Bandyopadhyay, E. J. Chun, and R. Mandal (2020), 2005.13933.
- [19] G. Bertone, D. Hooper, and J. Silk, Phys. Rept. **405**, 279 (2005), hep-ph/0404175.
- [20] L. Bian and Y.-L. Tang, JHEP **12**, 006 (2018), 1810.03172.
- [21] L. J. Hall, K. Jedamzik, J. March-Russell, and S. M. West, JHEP **03**, 080 (2010), 0911.1120.
- [22] K. Kajantie, M. Laine, K. Rummukainen, and M. E. Shaposhnikov, Nucl. Phys. B **466**, 189 (1996), hep-lat/9510020.
- [23] G. Giudice, A. Notari, M. Raidal, A. Riotto, and A. Strumia, Nucl. Phys. B **685**, 89 (2004), hep-ph/0310123.

- [24] A. Salvio, P. Lodone, and A. Strumia, JHEP **08**, 116 (2011), 1106.2814.
- [25] M. Laine and Y. Schroder, JHEP **02**, 068 (2012), 1112.1205.
- [26] S. Biondini, N. Brambilla, M. A. Escobedo, and A. Vairo, JHEP **12**, 028 (2013), 1307.7680.
- [27] B. Garbrecht, F. Glowna, and M. Herranen, JHEP **04**, 099 (2013), 1302.0743.
- [28] M. Laine, JHEP **08**, 138 (2013), 1307.4909.
- [29] A. Anisimov, D. Besak, and D. Bodeker, JCAP **03**, 042 (2011), 1012.3784.
- [30] D. Besak and D. Bodeker, JCAP **03**, 029 (2012), 1202.1288.
- [31] I. Ghisoiu and M. Laine, JCAP **12**, 032 (2014), 1411.1765.
- [32] A. Pilaftsis, Phys. Rev. D **56**, 5431 (1997), hep-ph/9707235.
- [33] A. Pilaftsis and T. E. Underwood, Nucl. Phys. B **692**, 303 (2004), hep-ph/0309342.
- [34] M. Flanz, E. A. Paschos, and U. Sarkar, Phys. Lett. B **345**, 248 (1995), [Erratum: Phys.Lett.B 384, 487–487 (1996), Erratum: Phys.Lett.B 382, 447–447 (1996)], hep-ph/9411366.
- [35] L. Covi, E. Roulet, and F. Vissani, Phys. Lett. B **384**, 169 (1996), hep-ph/9605319.
- [36] T. Frossard, M. Garny, A. Hohenegger, A. Kartavtsev, and D. Mitrouskas, Phys. Rev. D **87**, 085009 (2013), 1211.2140.
- [37] P. Bhupal Dev, P. Millington, A. Pilaftsis, and D. Teresi, Nucl. Phys. B **886**, 569 (2014), 1404.1003.
- [38] P. Bhupal Dev, P. Millington, A. Pilaftsis, and D. Teresi, Nucl. Phys. B **891**, 128 (2015), 1410.6434.
- [39] L. Lello, D. Boyanovsky, and R. D. Pisarski, Phys. Rev. D **95**, 043524 (2017), 1609.07647.
- [40] T. Hambye and D. Teresi, Phys. Rev. Lett. **117**, 091801 (2016), 1606.00017.
- [41] J. Ghiglieri and M. Laine, JCAP **07**, 015 (2016), 1605.07720.
- [42] J. Ghiglieri and M. Laine, JHEP **05**, 132 (2017), 1703.06087.
- [43] J. Ghiglieri and M. Laine, JHEP **02**, 014 (2019), 1811.01971.
- [44] G. Jackson and M. Laine, Nucl. Phys. B **950**, 114870 (2020), 1910.12880.
- [45] Y.-L. Tang (2019), 1908.09796.
- [46] A. Anisimov, D. Besak, and D. Bodeker, JCAP **03**, 042 (2011), 1012.3784.
- [47] P. Aurenche, F. Gelis, and H. Zaraket, JHEP **05**, 043 (2002), hep-ph/0204146.
- [48] S. Caron-Huot, Phys. Rev. D **79**, 065039 (2009), 0811.1603.
- [49] J. Chen, T. Han, and B. Tweedie, JHEP **11**, 093 (2017), 1611.00788.
- [50] M. L. Bellac, *Thermal Field Theory*, Cambridge Monographs on Mathematical Physics

- (Cambridge University Press, 2011), ISBN 9780511885068, 9780521654777, URL <http://www.cambridge.org/mw/academic/subjects/physics/theoretical-physics-and-mathematical>
- [51] M. D’Onofrio, K. Rummukainen, and A. Tranberg, Phys. Rev. Lett. **113**, 141602 (2014), 1404.3565.
 - [52] The International Linear Collider Technical Design Report - Volume 1: Executive Summary (2013), 1306.6327.
 - [53] The International Linear Collider Technical Design Report - Volume 2: Physics (2013), 1306.6352.
 - [54] The International Linear Collider Technical Design Report - Volume 3.I: Accelerator in the Technical Design Phase (2013), 1306.6353.
 - [55] The International Linear Collider Technical Design Report - Volume 3.II: Accelerator Baseline Design (2013), 1306.6328.
 - [56] H. Abramowicz et al., The International Linear Collider Technical Design Report - Volume 4: Detectors (2013), 1306.6329.
 - [57] CEPC Study Group (2018), 1809.00285.
 - [58] CEPC Study Group (2018), 1811.10545.
 - [59] A. Abada et al. (FCC), Eur. Phys. J. ST **228**, 261 (2019).
 - [60] F. F. Deppisch, P. Bhupal Dev, and A. Pilaftsis, New J. Phys. **17**, 075019 (2015), 1502.06541.
 - [61] S. Antusch, E. Cazzato, and O. Fischer, JHEP **12**, 007 (2016), 1604.02420.
 - [62] S. Antusch, E. Cazzato, and O. Fischer, Int. J. Mod. Phys. A **32**, 1750078 (2017), 1612.02728.
 - [63] P. Hernández, J. Jones-Pérez, and O. Suarez-Navarro, Eur. Phys. J. C **79**, 220 (2019), 1810.07210.
 - [64] Z. S. Wang and K. Wang, Phys. Rev. D **101**, 075046 (2020), 1911.06576.
 - [65] M. S. Chanowitz and M. K. Gaillard, Nucl. Phys. **B261**, 379 (1985).